

# Probing the Structural/Electronic Diversity and Thermal Stability of Various Nanocrystalline Powders of Gallium Nitride GaN

Mariusz Drygas,<sup>†</sup> Zbigniew Olejniczak,<sup>‡</sup> Ewa Grzanka,<sup>§</sup> Mirosław M. Bucko,<sup>||</sup>  
Robert T. Paine,<sup>⊥</sup> and Jerzy F. Janik<sup>\*†</sup>

Faculty of Fuels and Energy and Faculty of Materials Science and Ceramics, AGH University of Science and Technology, al. Mickiewicza 30, 30-059 Krakow, Poland, Institute of Nuclear Physics, Polish Academy of Sciences, ul. Radzikowskiego 152, 31-342 Krakow, Poland, Institute of High Pressure Physics, Polish Academy of Sciences, ul. Sokolowska 29/37, 01-142 Warszawa, Poland, and Department of Chemistry, University of New Mexico, Albuquerque, New Mexico 87131

Received March 5, 2008. Revised Manuscript Received July 29, 2008

Nineteen different gallium nitride nanopowders were prepared with four distinct synthesis methods under a wide range of experimental conditions. Variations of synthetic details were aimed at making diverse GaN powders, mainly, from a viewpoint of their structural and thermal stability properties. The supplemental application of powder XRD and <sup>69</sup>Ga MAS NMR spectroscopic methods enabled a coherent insight into both the long-range structural order and electronic features, respectively, supporting the specific Knight shift effect displayed in the NMR spectra of the powders. Thermogravimetric measurements under a neutral gas atmosphere were conducted to probe stability ranges of the powders. The combined results support a broad diversity of GaN nanopowders that require supplemental characterization methods to satisfactorily define their complex structural, compositional, and electronic properties evolved during high-temperature syntheses or thermal annealing.

## Introduction

The utilization of powder forms of many new materials including semiconducting gallium nitride GaN is far from satisfactory despite significant progress in the development of relevant synthetic methods.<sup>1</sup> One of the attractive applications to consider is powder sintering into mechanically robust and machinable ceramics that could be a material of choice, for instance, for an economical replacement of GaN single-crystal supports in optoelectronics. Preliminary reports on the high-temperature high-pressure sintering of nano-GaN powders highlighting selected follow-up applications of the resulting ceramics have been published elsewhere.<sup>2</sup> The crucial conclusion from these efforts based on examination of the GaN ceramic quality was a challenging need for the reproducible and unequivocally characterized powder feed-

stock, a limiting factor in successful optimization of the sintering process.

Powder XRD has been a key method for structure elucidation of GaN crystalline powders. However, estimations of even such common parameters as average crystallite sizes and lattice parameters can be severely misinterpreted for nanopowders if standard calculation tools that have been derived for microcrystalline systems are applied.<sup>3</sup> In addition, gallium nitride is known to exhibit a range of defected hexagonal structures in the nanosized region. Furthermore, GaN can tolerate a rather undefined extent of nitrogen deficiency vs the ideal 1/1 Ga/N ratio, with the latter feature having an undetermined impact on grain crystallinity. All this makes standard XRD data for nanocrystalline GaN powders highly equivocal.

The ambiguity of the XRD data for a limited number of such powders has been substantiated by supplemental <sup>69</sup>Ga or <sup>71</sup>Ga MAS NMR measurements that in principle probe short-range chemical environments of gallium centers in both hexagonal GaN<sup>4–6</sup> and cubic GaN<sup>5</sup> powders, as stressed

\* Corresponding author. E-mail: janikj@agh.edu.pl.

<sup>†</sup> Faculty of Fuels and Energy, AGH University of Science and Technology.

<sup>‡</sup> Institute of Nuclear Physics, Polish Academy of Sciences.

<sup>§</sup> Institute of High Pressure Physics, Polish Academy of Sciences.

<sup>||</sup> Faculty of Materials Science and Ceramics, AGH University of Science and Technology.

<sup>⊥</sup> University of New Mexico.

- (1) (a) Janik, J. F. *Powder Technol.* **2005**, *152*, 118. (b) Gubin, S. P.; Kataeva, N. A.; Khomutov, G. B. *Russ. Chem. Bull., Int. Ed.* **2005**, *54* (4), 827. (c) Trindade, T.; O'Brien, P.; Pickett, N. L. *Chem. Mater.* **2001**, *13*, 3843.
- (2) (a) Stelmakh, S.; Swiderska-Sroda, A.; Kalisz, G.; Gierlotka, S.; Grzanka, E.; Palosz, B.; Drygas, M.; Janik, J. F.; Paine, R. T. *Proceedings of the International Conference on Nanoscience and Technology*, Basel, Switzerland, July 30–August 4, 2006; Institute of Physics Publishing: Philadelphia, PA, 2006; Poster 1399. (b) Grzanka, E.; Stelmakh, S.; Gierlotka, S.; Swiderska-Sroda, A.; Kalisz, G.; Palosz, B.; Drygas, M.; Janik, J. F.; Paine, R. T. Presented at the European Powder Diffraction Conference, EPDIC-10, Geneva, Switzerland, Sept 1–4, 2006; *Z. Kristallogr.*, **2007**, *26*, MS11-P92. (c) Borysiuk, J.; Caban, P.; Strupinski, W.; Gierlotka, S.; Stelmakh, S.; Janik, J. F. *Cryst. Res. Technol.* **2007**, *42* (12), 1291.

- (3) (a) Palosz, B.; Grzanka, E.; Gierlotka, S.; Stelmakh, S.; Pielaszek, R.; Lojkowski, W.; Bismayer, U.; Neufeind, J.; Weber, H. P.; Palosz, W. *Phase Transitions, Part B* **2003**, *76* (1–2), 171. (b) Petkov, V.; Gatashki, M.; Choi, J.; Gillan, E. G.; Ren, Y. *J. Mater. Chem.* **2005**, *15*, 4654. (c) Tamas, U.; Gubicza, J. *Z. Kristallogr.* **2007**, *222*, 114.
- (4) (a) Han, O. H.; Timken, H. K. C.; Oldfield, E. *J. Chem. Phys.* **1988**, *89* (10), 6046. (b) Jung, W.-S.; Park, C.; Han, S. *Bull. Korean Chem. Soc.* **2003**, *24* (7), 1011. (c) Jung, W.-S. *Mater. Lett.* **2006**, *60*, 2954. (d) Schwenzer, B.; Hu, J.; Seshadri, R.; Keller, S.; DenBaars, S. P.; Mishra, U. K. *Chem. Mater.* **2004**, *16*, 5088. (e) Schwenzer, B.; Hu, J.; Wuc, Y.; Mishra, U. K. *Solid State Sci.* **2006**, *8*, 1193.
- (5) (a) Yesinowski, J. P.; Purdy, A. P. *J. Am. Chem. Soc.* **2004**, *126*, 9166. (b) Jung, W.-S.; Han, O. H.; Chae, S.-A. *Mater. Chem. Phys.* **2006**, *100*, 199.

originally in studies by W.-S. Jung et al.<sup>4b,c</sup> and B. Schwenzer et al.<sup>4d,e</sup> In the case of hexagonal GaN, especially for GaN powders obtained in the 1000–1100 °C range from ammonolysis of oxygen-bearing gallium precursors, the well-defined hexagonal pattern for h-GaN in its XRD scan has been associated with a usually minor resonance at ca. 330 ppm in the respective gallium NMR spectrum. In contrast, a major broad NMR line at ca. 400–450 ppm has been linked by a few researchers to a structurally undefined nitrogen deficient phase or impurity (O. H. Han,<sup>4a</sup> W.-S. Jung,<sup>4b,c</sup> B. Schwenzer<sup>4d,e</sup>). In only one study known to us, a few high-temperature made Ga<sup>15</sup>N powders have been shown by XRD to display a rather unusual double hexagonal pattern, suggesting the existence of two different h-GaN phases.<sup>4d,e</sup> Some of these powders exhibited a sharp resonance at 330 ppm in the <sup>71</sup>Ga MAS NMR spectrum accompanied by a broad resonance with shoulders in the 350–500 ppm range. Similarly shaped resonances were also observed in the respective <sup>15</sup>N MAS NMR spectrum. The existence of two hexagonal phases and the presence of two sets of the correlated multinuclear NMR resonances were proposed as an argument for the crystalline (hexagonal) character of the distinct N-deficient phase.

In an alternative breakthrough proposal, the Knight shift due to conduction electrons in a semiconductor has been proposed by Yesinowski and co-workers to account for the second high-frequency peak shifting and broadening in the gallium MAS NMR spectra for at least some GaN powders, especially those intentionally doped and/or containing impurities even at low levels of a few tenths of a percent.<sup>5a,6</sup> This well-substantiated approach stresses the importance of electronic factors due to dopant (intentional or unintentional) related conduction electrons over purely short-range chemical environment effects and is also consistent with the single pattern for h-GaN in most of the corresponding XRD spectra.

It should not be surprising that the structural ambiguities for GaN powders outlined above have high relevance to their thermal stabilities. In a majority of synthesis methods, especially those based on nitridation of oxygen-bearing gallium precursors, the required pyrolysis temperatures are in the 950–1000 °C and higher range, which also happens to be a stability threshold for GaN. Additionally, in such a temperature regime, recrystallization and sublimation phenomena are known to reach noticeable levels. It is therefore clear that from the viewpoint of high-temperature GaN powder applications progressing decomposition phenomena have to be especially appraised. In this regard, thermogravimetric methods seem to conveniently and adequately address the powder stability issue.<sup>7</sup>

Herein, we report investigations of structural, electronic, and stability properties for a diverse range of GaN nanopowders.

They were prepared with several processing conditions by using four different synthesis methods thus providing an unparalleled set of materials. Powder XRD and <sup>69</sup>Ga MAS NMR spectroscopy occasionally supplemented with XPS determinations were used for structural assignments. In this regard, if the peak resolution is not of major concern (significant distances between resonance frequencies), both the <sup>69</sup>Ga and <sup>71</sup>Ga NMR experiments provide qualitatively matched and quantitatively comparable results while the observed peak positions usually vary by a few parts per million. Because the resonance frequencies in GaN for the observed species differ by some plus 100 ppm, even with the significant peak broadness one gets satisfactory data resolution from the <sup>69</sup>Ga NMR experiment. TGA/DTA studies under an UHP helium atmosphere were carried out to evaluate powder stabilities at elevated temperatures. For several samples, residual oxygen contents were also determined to estimate the completeness of nitridation.

## Experimental Section

**Preparation.** Four distinct synthesis routes were applied to make GaN powders. (i) A two-stage aerosol-assisted method utilized aqueous or DMF solutions of gallium nitrate Ga(NO<sub>3</sub>)<sub>3</sub>·xH<sub>2</sub>O (Strem Chemicals).<sup>8</sup> First, an aerosol mist of the solution was injected into a ceramic tubular reactor where it mixed with an ammonia-rich atmosphere at 1000–1100 °C under specific process conditions to yield a raw aerosol powder with an average composition Ga<sub>2</sub>O<sub>3</sub>N<sub>z</sub>. This stage was followed by pyrolysis of the raw powders at a selected temperature in the 900–1000 °C range under an ammonia flow, 0.2 L/min, producing gray-yellowish materials. It is worth noting that the pyrolysis experiments resulted also in the formation of substantial quantities of black deposits at the reactor's cold exit. In two separate cases, the first stage was carried out under a neutral nitrogen atmosphere at 400 or 1050 °C to yield aerosol-generated Ga<sub>2</sub>O<sub>3</sub> as raw powders that were later pyrolyzed in the second stage under an ammonia flow resulting in severely agglomerated GaN bodies. In one case, the first stage was conducted with a dimethylformamide (DMF) solution of gallium nitrate. Furthermore, one first-stage experiment was carried out in an Inconel tube reactor to check for a possible impact of metal-containing reaction environment on the raw powder generation. One product powder was additionally cleaned by treatment with a 5% aqueous solution of HF for 20 h. (ii) The nitriding conversions of commercial (Aldrich) and aerosol-generated Ga<sub>2</sub>O<sub>3</sub> powders (see above) were done in ceramic crucibles under an ammonia flow, 0.2 L/min, by setting an appropriate temperature in the 900–975 °C range and, typically, 6 or 12 h time of pyrolysis. Products were grayish yellow to dark gray powders. (iii) The anaerobic method employed the pyrolysis of freshly synthesized gallium imide at 600, 700, and 975 °C under an ammonia flow of 0.2 L/min as already published.<sup>9</sup> The pyrolyses at 700 and 975 °C were followed by 1 h evacuation at the pyrolysis temperature before cooling to ambient temperature. The products were yellow to gray powders. (iv) The nitriding pyrolyses of powdered monocrySTALLINE gallium arsenide GaAs (a generous gift of Dr. Slupinski, Institute of Experimental Physics, Warsaw University, Warsaw, Poland) were done at 700

(6) (a) Yesinowski, J. P. *Phys. Status Solidi C* **2005**, 2 (7), 2399. (b) Yesinowski, J. P.; Purdy, A. P.; Wu, H.; Spencer, M. G.; Hunting, J.; DiSalvo, F. J. *J. Am. Chem. Soc.* **2006**, 128, 4952. (7) (a) Groh, R.; Gerey, G.; Bartha, L.; Pankove, J. I. *Phys. Status Solidi A* **1974**, 26, 353. (b) Li, J. Y.; Chen, X. L.; Qiao, Z. Y.; Cao, Y. G.; Lan, Y. C. *J. Cryst. Growth* **2000**, 213, 408. (c) Xiao, H.-D.; Ma, H.-L.; Lin, Z.-J.; Ma, J.; Zong, F.-J.; Zhang, X.-J. *Mater. Chem. Phys.* **2007**, 106, 5. (d) Unland, J.; Onderka, B.; Davydov, A.; Schmid-Fetzer, R. *J. Cryst. Growth* **2003**, 256, 33.

(8) (a) Wood, G. L.; Pruss, E. A.; Paine, R. T. *Chem. Mater.* **2001**, 13, 12. (b) Janik, J. F.; Drygas, M.; Stelmakh, S.; Grzanka, E.; Palosz, B.; Paine, R. T. *Phys. Status Solidi A* **2006**, 203 (6), 1301. (9) (a) Janik, J. F.; Wells, R. L. *Chem. Mater.* **1996**, 8, 2708. (b) Wells, R. L.; Janik, J. F.; Gladfelder, W. L.; Coffey, J. L.; Johnson, M. A.; Steffey, B. D. *Mater. Res. Soc. Symp. Proc.* **1997**, 468, 39.

**Table 1. Summary of Synthesis Methods and Resulting Gallium Nitride GaN Powders<sup>a</sup> (Residual Oxygen Contents for Powders, O, x wt %, Are Shown, If Available)**

synthesis method			
aerosol-assisted: stage 1//stage 2	Ga <sub>2</sub> O <sub>3</sub> nitridation	anaerobic	GaAs nitridation
A1 (1000/H <sub>2</sub> O//1000/6); O, 0.4 wt %; gray	B1 (comm/900/12); O, 4.2 wt %; l. yellow	C1 (600/16); yellow	D1 (700/150/slow); gray-beige
A2 (1050/H <sub>2</sub> O/Inconel//1000/8); gray-beige			
A3 (1050/DMF//975/6); d. gray	B2 (comm/950/12); O, 1.7 wt %; gray	C2 (700/4/vac); yellow-gray	D2 (800/90/slow); gray-beige
A4 (1050/H <sub>2</sub> O//975/6); O, 1.9 wt %; l. gray			
A5 (1100/H <sub>2</sub> O//900/6); O, 4.5 wt %; yellow	B3 (comm/975/12); O, 1.3 wt %; d. gray	C3 (975/4/vac); gray	D3 (800/90/fast); gray-beige
A6 (1100/H <sub>2</sub> O//950/6); O, 2.9 wt %; yellow			
A7 (1100/H <sub>2</sub> O//1000/6); O, 2.1 wt %; l. gray	B4 (aero/400//975/6); gray-beige		
A8 (1100/H <sub>2</sub> O//975/6/HF); O, 2.1 wt % before HF treatment; l. gray	B5 (aero/1050//975/6); O, 3.8 wt %; l. gray		

<sup>a</sup> In parentheses: (i) samples A—*aerosol generation temperature (°C)/solvent/pyrolysis temperature (°C)/pyrolysis time (h)*; the Inconel tube (A2) and HF washing (A8) experiments are indicated; (ii) samples B—*comm/(commercial)/pyrolysis temperature (°C)/pyrolysis time (h)*; *aero* (aerosol-generated)/*aerosol generation temperature (°C)/pyrolysis temperature (°C)/pyrolysis time (h)*; (iii) samples C—*pyrolysis temperature (°C)/pyrolysis time (h)/vacuum applied during last hour of pyrolysis*; (iv) samples D—*pyrolysis temperature (°C)/pyrolysis time (h)/relative NH<sub>3</sub> flow rate*.

°C for 150 h and at 800 °C for 90 h under a NH<sub>3</sub> flow. At a given pyrolysis temperature, a choice of pyrolysis time and flow rate of NH<sub>3</sub> were crucial to complete nitridation; otherwise, some residual c-GaAs persisted.<sup>5b</sup> The products were gray-beige tinted powders. All GaN powders are summarized in Table 1. The sample names include crucial synthesis parameters shown in the parentheses (see Table 1 footnotes).

**Characterization.** All products were characterized by standard powder XRD spectroscopy (Siemens D5000 or X'Pert Pro Analytical with Cu K $\alpha$  source;  $2\theta = 20\text{--}80^\circ$ ). Average crystallite sizes were evaluated from Scherrer's equation applying the Rietveld refinement method. For the evaluation, changes of the line profile parameters compared to a standard sample were utilized. Our standard was a polycrystalline alumina sintered body with an average grain size over 5  $\mu\text{m}$  subjected to stress relief annealing. The profile parameters depend on the instrument settings used for data collection and on the profile function used for the refinement. In our analysis the full Voigt function was used to describe the profile of the measured diffraction lines. The total profile width is a convolution of the Gaussian profile part and of the Lorentzian profile part and these parts are combined numerically. In such a method, the full width at half-maximum (fwhm) is only one of a few fitted parameters. Solid-state MAS NMR spectra of <sup>69</sup>Ga nuclei were measured on the APOLLO console (Tecmag) at the magnetic field of 7.05 T produced by the 89 mm bore superconducting magnet (Magnex). A Bruker HP-WB high-speed MAS probe equipped with the 4 mm zirconia rotor and KEL-F cap was used to record the MAS spectra at the spinning rate ranging from 7 to 9 kHz. The spectra were measured at 71.925 MHz using a single 2  $\mu\text{s}$  rf pulse, which corresponded to  $\pi/4$  flip angle in the liquid. The acquisition delay used in accumulation was 1 s and the typical number of acquisitions was equal to 1000. The frequency scale in ppm was referenced to the <sup>69</sup>Ga resonance in the 1.1 M solution of Ga(NO<sub>3</sub>)<sub>3</sub> in heavy water. All peak positions are reported as observed shifts not corrected for the second-order quadrupolar shifts. Note that for the purpose of convenient presentation, the spectra are displayed in the normalized mode. To identify the spinning sidebands appearing in some spectra, we measured the selected samples at two spinning rates, i.e., 7 and 9 kHz. Because of limited bandwidths of the MAS probe and the NMR receiver, the signal from metallic gallium had to be searched by a systematic change of the resonance offset in the NMR console, paralleled by the corresponding retuning of the probe. Once the NMR signal from the metallic  $\beta$ -Ga was detected at the 0.45% Knight shift (no signal was detected in the Knight shift range expected for  $\alpha$ -Ga),<sup>10</sup> the

NMR spectrum was measured using the same acquisition parameters as in the normal frequency range. XPS data were determined with a Vacuum System Workshop Ltd. instrument primarily equipped with a Al K $\alpha$  X-ray radiation source (1486.6 eV, 200 W) and spectral energies were referenced relative to carbon (284.6 eV). Because for the Al-source strong Auger lines appeared to severely overlap the N 1 s band, a Mg K $\alpha$  (1253.6 eV) radiation source was used to record and refine the nitrogen spectrum. TGA/DTA determinations were carried out on the TA-Instruments STA-SDT 2960 apparatus (disposable Al<sub>2</sub>O<sub>3</sub> crucibles, helium UHP 5N, sample mass 50–80 mg, helium purge before determinations at 30 °C for 1 h, practical temperature range 40–1100 °C, heating rate 10 °C/min). For selected materials, residual oxygen contents were determined (Saint-Gobain/Carborundum Corp. Boron Nitride, Amherst, NY).

## Results and Discussion

**Synthesis Methods and Powder Products.** *Aerosol-Assisted Synthesis.* The convenient and highly automated aerosol-assisted synthesis method starts with the affordable gallium nitrate precursor yielding a unique spherical particle morphology of GaN.<sup>8</sup> In this case, the utilization of the oxygen-bearing precursor results in product powders after pyrolysis in the optimal 975–1000 °C range with residual oxygen contents up to 1–2 wt %, average crystallite size range typically above 25–30 nm, and crystallites shown by XRD to have good-quality hexagonal structure.<sup>8b</sup> By a suitable adjustment of experimental conditions, oxygen contents below 1 wt % are attainable.

It is worth noting that after several second-stage pyrolysis runs, substantial quantities of a sootlike black deposit are observed at the tube reactor's cold exit. Figure 1 presents from left to right the XRD scan, <sup>69</sup>Ga MAS NMR spectrum in the metallic  $\beta$ -Ga range, and XPS Ga 3d band for the deposit. The XRD data support the complex composition of the material to include mainly gallium oxide  $\beta$ -Ga<sub>2</sub>O<sub>3</sub>, hexagonal gallium nitride GaN, metallic gallium Ga, and a minor undetermined component with a probable spinel-like phase. This should be compared with the NMR evidence for metallic  $\beta$ -Ga (Knight shift at +0.45%);<sup>10</sup> in this case, the instrument's characteristics ruled out a detection of severely broadened resonances for Ga<sub>2</sub>O<sub>3</sub>. Finally, the XPS spectrum is consistent with the presence of the prevailing Ga<sub>2</sub>O<sub>3</sub>, minor GaN, and some metallic Ga.

(10) (a) Stroud, J. D.; Segel, S. L. *J. Phys. F: Metal Phys.* **1975**, *5*, 1981.  
(b) Cornell, D. A. *Phys. Rev.* **1967**, *153* (1), 208.

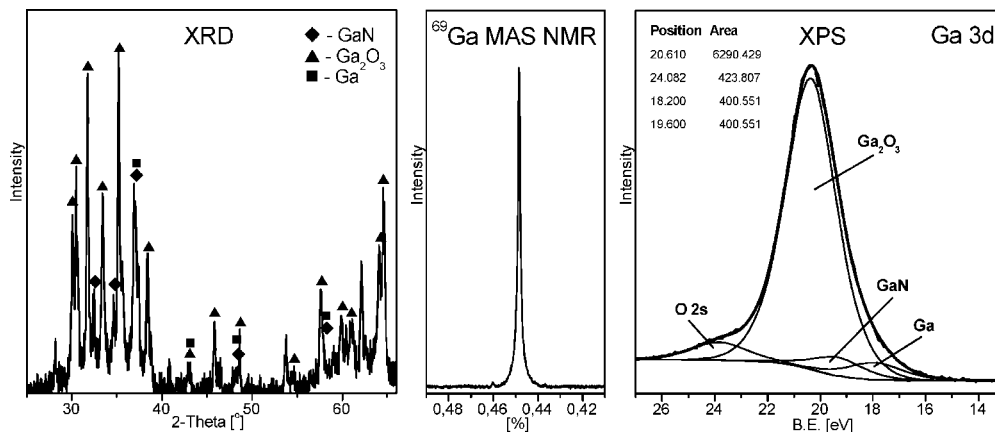


**Figure 1.** From left to right: XRD pattern, <sup>69</sup>Ga MAS NMR spectrum in the  $\beta$ -Ga Knight shift range, and XPS Ga 3d band for the black byproduct deposit in aerosol-assisted method.

In all likelihood, these deposits condense from the vapor phase upon gas stream cooling down at the reactor's cold exit. The occurrence of the practically nonvolatile oxide and metal at the far end from the crucible suggests their formation from disproportionation of the volatile and unstable gallium suboxide according to  $3\text{Ga}_2\text{O} \rightarrow \text{Ga}_2\text{O}_3 + 4\text{Ga}$ , whereas a gas phase ammonolysis of the suboxide would yield GaN from  $\text{Ga}_2\text{O} + 2\text{NH}_3 \rightarrow 2\text{GaN} + \text{H}_2\text{O} + 2\text{H}_2$ .<sup>11</sup> In this regard, the likely formation of the suboxide would involve the reaction between not yet nitrated Ga<sub>2</sub>O<sub>3</sub> in the raw Ga<sub>x</sub>O<sub>y</sub>N<sub>x</sub> powder and metallic Ga,<sup>12</sup> the latter originating from a concurrent at this temperature range decomposition of GaN or, alternatively, from oxide reduction with hydrogen from ammonia decomposition.<sup>13</sup> As a matter of fact, noticeable metallic gallium was sometimes observed on the crucible's bottom after prolonged nitriding conversions at 975–1000 °C. These observations confirm that complex and competing reactions take place during the nitriding pyrolysis of oxygen-bearing gallium precursors and fine process tuning is required to maximize the target reaction.

The case of aerosol generation employing the Inconel reactor resulted in a small yield of a black powder that by XRD spectroscopy (not shown) contained mostly nanocrystalline  $\gamma$ -Ga<sub>2</sub>O<sub>3</sub>. The black color of the product also implied some metallic gallium, thus supporting significant reduction chemistry operating in this system, likely enhanced by the metallic reactor via extensive ammonia decomposition and increased hydrogen concentrations. Upon subsequent nitriding pyrolysis at 1000 °C, a gray-beige tinted powder, A2, was produced.

**Nitridation of Ga<sub>2</sub>O<sub>3</sub>.** The straightforward nitridation of gallium oxide powder with ammonia at 950–1000 °C also yields hexagonal GaN powders with up to 2 wt % residual oxygen contents. As typical for nitriding conversion of oxygen containing Ga-precursors, the necessity of high temperatures and long pyrolysis times promoted quite extensive powder losses due to simultaneously occurring GaN decomposition and sublimation processes. The condensation of black deposits was also observed. Samples B1–

B3 in Table 1 well-illustrate the effect of temperature on the residual O content in the products made from the commercial source and suggest the 950–975 °C pyrolysis range as optimal to yield powders with O contents below 2 wt %.

A different picture emerges from nitriding of Ga<sub>2</sub>O<sub>3</sub> aerosol powders prepared earlier via aerosol-assisted decomposition of gallium nitrate solutions (samples B4 and B5). On the basis of the XRD scans (not shown), the homemade aerosol Ga<sub>2</sub>O<sub>3</sub> powder prepared at 400 °C was nanocrystalline  $\gamma$ -Ga<sub>2</sub>O<sub>3</sub> and the powder prepared at 1050 °C was the common  $\beta$ -Ga<sub>2</sub>O<sub>3</sub> polytype. The subsequent nitriding pyrolyses of these powders at 975 °C resulted in severely sintered products. It appears that ammonolysis of such Ga<sub>2</sub>O<sub>3</sub> powders proceeds through an undesirable agglomeration stage that results in poor nitridation conversions, which is evidenced by higher residual oxygen contents than in the comparable cases of commercial Ga<sub>2</sub>O<sub>3</sub> nitridation, e.g., 3.8 vs 1.3 wt % for powders B5 and B3, respectively.

**Anaerobic Synthesis.** The anaerobic synthesis of GaN from pyrolysis of gallium imide has the advantage of providing powders with minimal if any oxygen contents and with ample room for temperature-controlling crystallite sizes in the low nanometer range down to a few nanometers, which is unattainable by other methods in this study.<sup>9</sup> Residual C contents (not analyzed) are expected to be very small, very often below the detection limits of ca. 0.1% of standard combustion methods.<sup>9a</sup> In this process, very reactive powders of mostly defected hexagonal GaN polytype are produced with high specific surface area and attractive adsorption properties stemming from surface derivatization with imide/amide/ammonia functionalities.<sup>14</sup> To minimize postreaction ammonia adsorption, we carried out some preparations in this study with an additional step of applying a dynamic vacuum in the last hour of pyrolysis.

**Nitridation of GaAs.** A specific feature of the nitriding conversion of cubic gallium arsenide GaAs in the 700–900 °C range is the production of GaN powder being a mixture of the predominant cubic variety (zinc blende) and the minor hexagonal polytype (defected) in the lowest microcrystalline

(11) Balkas, C. M.; Davis, R. F. *J. Am. Ceram. Soc.* **1996**, 79 (9), 2309.

(12) (a) Brukl, D. A. *Z. Anorg. Allg. Chem.* **1932**, 203, 23. (b) Frosch, C. J.; Thurmond, C. D. *J. Phys. Chem.* **1962**, 66 (5), 877.

(13) Butt, D. P.; Park, Y.; Taylor, T. N. *J. Nucl. Mater.* **1999**, 264, 71.

(14) Czepirski, L.; Janik, J. F.; Komorowska-Czepirska, E.; Wells, R. L. *Adsorpt. Sci. Technol.* **2002**, 20 (8), 723.

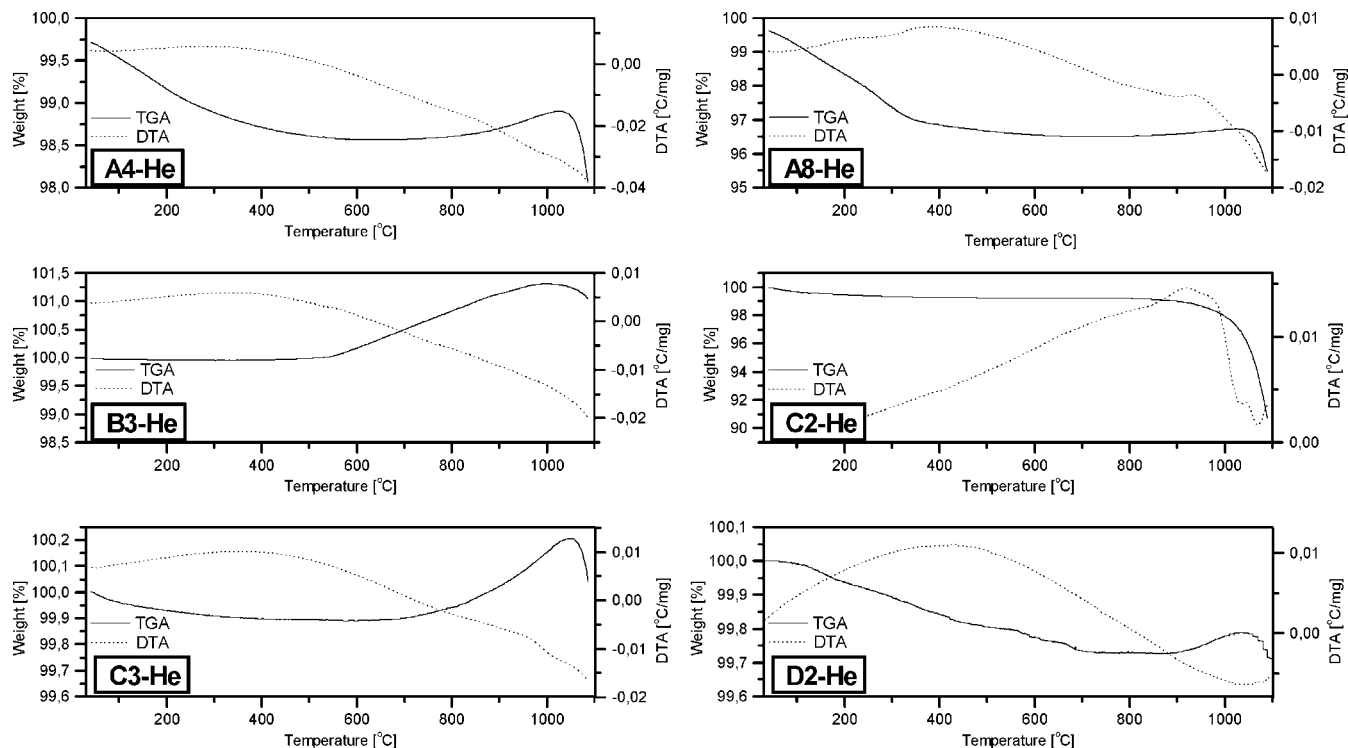


Figure 2. TGA/DTA curves under UHP helium for selected GaN powders.

Table 2. Weight Changes and Characteristic Temperatures in the Heating of GaN Powders under UHP Helium in TGA/DTA Experiments<sup>a</sup>

powder	weight loss (wt %) below $T_1$ ( $<T_1$ )	weight increase (wt %) in the range $T_2$ – $T_{\text{decomp}}$	temperature of GaN decomposition
A4	1.1 ( $<500$ °C)	0.2 (500–1020 °C)	1020 °C
A8	3.1 ( $<350$ °C)	0.2 (700–1020 °C)	1020 °C
B3	$<0.1$ ( $<400$ °C)	1.3 (500–1000 °C)	1000 °C
C2	0.8 ( $<300$ °C)	continuous weight loss	930 °C (850 °C)
C3	0.1 ( $<400$ °C)	0.3 (700–1050 °C)	1050 °C
D2	0.3 ( $<730$ °C)	0.1 (850–1040 °C)	1040 °C

<sup>a</sup>  $T_1$ , temperature to which initial weight loss continues;  $T_2$ , temperature from which weight increase starts;  $T_{\text{decomp}}$ , temperature of abrupt GaN decomposition.

range.<sup>5b</sup> Such powders may under unfavorable experimental circumstances contain traces of residual GaAs. In this regard, the importance of the rate of ammonia flow is illustrated by the properties of related samples D2 and D3. Here, the formation of the prevailing rare cubic polytype of GaN can be envisioned as resulting from advantageous topochemical conditions set up by the cubic lattice of the GaAs substrate.

**Thermal Stabilities of Powders.** The TGA/DTA traces under UHP helium for six selected GaN powders are shown in Figure 2 and derived characteristic parameters are displayed in Table 2. All materials show an initial weight loss below  $T_1$  (300–730 °C). Subsequently, five of the materials (excluding C2, which shows a continuous weight loss) show a weight increase beginning at  $T_2$  (500–850 °C) that terminates with an abrupt weight decrease around  $T_{\text{decomp}}$  at 930–1050 °C, the latter corresponding to rapid GaN decomposition. The low-temperature weight loss is due primarily to release of surface adsorbed postprocessing gases and possibly some surface reactive groups condensation byproducts. The observed slight weight increase at higher temperatures likely involves an oxidation effect because weight gain is predicted for oxidation of GaN. Apparently, some contaminant oxygen in the UHP helium is responsible for this effect. Although the TGA/DTA traces are qualitatively

similar, there are remarkable quantitative differences among the powders. The unusually high initial weight loss of 3.1 wt % for sample A8 as compared with the losses of the order of 0.1 wt % for powders B3 and C3 is worth noting. In this regard, powder A8 was additionally treated with an aqueous HF solution to remove oxide species and, apparently, significant quantities of H<sub>2</sub>O were concurrently adsorbed and/or chemisorbed on grain surfaces. Similar powder A4 that was not HF-treated shows a much lower 1.1 wt % loss at this stage. The low weight loss for powder B3 can be linked to the likely low surface area of this highly crystalline material and resulting smaller quantities of adsorbed species while for powder C3 the applied high-temperature evacuation after synthesis appears to remove most of the adsorbed postreaction gases.

From the viewpoint of powder stabilities, the TGA-determined decomposition temperatures span the range of 930–1050 °C. With the exception of powder C2 (anaerobic synthesis, pyrolysis at 700 °C) the remaining powders despite the different origin and phase properties (vide infra) show comparable thermal stabilities with decomposition temperatures in the close 1000–1050 °C range. In this regard, powder C2 with  $T_{\text{decomp}}$  at 930 °C (faster weight decrease due to decomposition already starts at ca. 850 °C) is

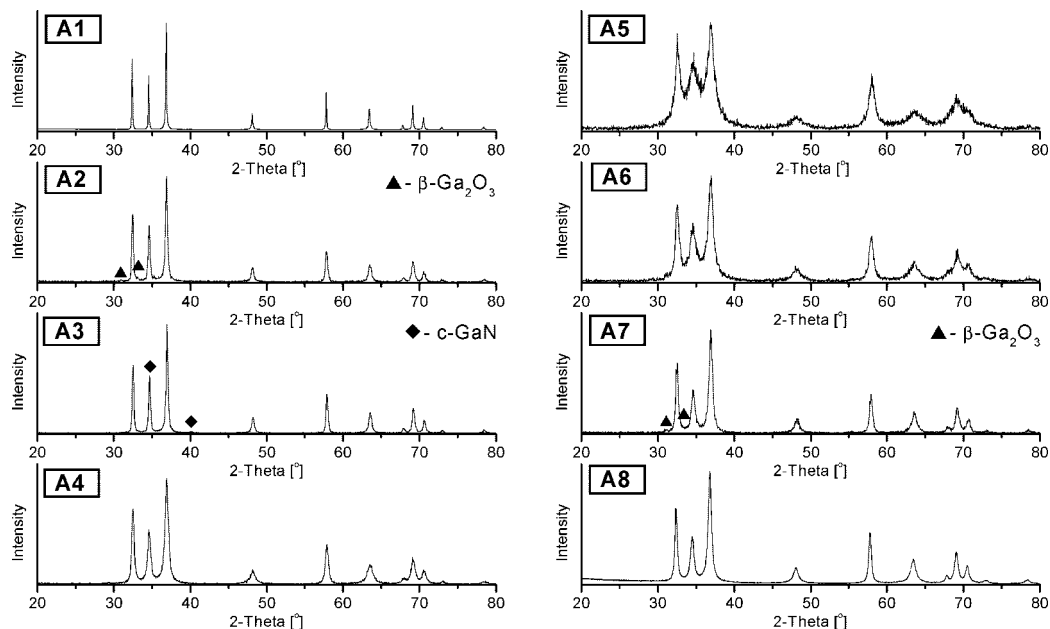


Figure 3. XRD patterns for GaN powders A1–A8 from aerosol-assisted synthesis.

Table 3. Crystalline Phase Analysis for GaN Powders A1–A8 from Aerosol-Assisted Synthesis ( $D$  ( $hkl$ ), Average Crystallite Size;  $a$  and  $c$ , Hexagonal Lattice Parameters)

	A1 (1000/H <sub>2</sub> O//1000/6)	A2 (1050/H <sub>2</sub> O/Inconel//1000/8)	A3 (1050/DMF//975/6)	A4 (1050/H <sub>2</sub> O//975/6)
major h-GaN (ordered):	v. sharp	sharp	sharp	sharp
$D$ (100) (nm)	190	56	62	29
$D$ (002) (nm)	140	44	50	19
$D$ (101) (nm)	100	39	46	18
$a$ (Å)	3.1893	3.1882	3.1888	3.1881
$c$ (Å)	5.1867	5.1850	5.1878	5.1892
residual c-GaN	no	no	2.5 wt %	no
residual G <sub>2</sub> O <sub>3</sub>	no	verge of detection	no	no
	A5 (1100/H <sub>2</sub> O//900/6)	A6 (1100/H <sub>2</sub> O//950/6)	A7 (1100/H <sub>2</sub> O//1000/6)	A8 (1100/H <sub>2</sub> O//975/6/HF)
major h-GaN (ordered):	v. broad	broad	sharp	sharp
$D$ (100) (nm)	11	15	27	31
$D$ (002) (nm)	5	7	14	20
$D$ (101) (nm)	7	10	18	21
$a$ (Å)	3.1834	3.1856	3.1872	3.188(2)
$c$ (Å)	5.1956	5.1917	5.1860	5.184(2)
residual c-GaN	no	no	no	no
residual G <sub>2</sub> O <sub>3</sub>	no	no	verge of detection	no

characterized with the smallest average grain size and GaN grains displaying defected hexagonal structure while the remaining powders have significantly larger grain sizes (vide infra). This suggests that the interplay of the somewhat correlated grain size and h-GaN structure inhomogeneity factors may be primarily responsible for the trend in decomposition temperatures with larger grains of usually better crystallinity showing overall higher stabilities.

At this point, it is worth indicating that the reported GaN decomposition temperatures span a wide range from below 800 °C (400 °C under H<sub>2</sub>) to higher than 1100 °C and depend on the applied conditions (vacuum, neutral or reactive gas atmosphere, time, specifics of detection technique) and the kind of GaN sample.<sup>7,13</sup> It is interesting to compare this range with the TGA-derived temperature of 930 °C used for intentional sublimation of the ball-milled GaN powders<sup>7b</sup> and 1120 °C decomposition temperature for microcrystalline powders from nitriding of Ga<sub>2</sub>O<sub>3</sub><sup>7c</sup> or 800 °C originally reported as GaN sublimation temperature under the pressure

of 1 atm.<sup>7a</sup> It is clear that in the 900–1100 °C range pertinent to our synthesis conditions, both sublimation and decomposition phenomena may take place enhanced by the nanosize dimensions of the powders.<sup>15</sup>

**Powder XRD Characterization.** Figure 3 includes the diffraction patterns for samples A1–A8 from the aerosol-assisted synthesis and derived structure data are shown in Table 3. The major product by XRD in all samples is a relatively well-ordered hexagonal GaN, h-GaN, with a range of average crystallite sizes. The calculated lattice parameters are in reasonable agreement with the values reported for crystalline h-GaN<sup>16</sup> (e.g., ref 16a:  $a = 3.189(1)$  Å,  $c = 5.185(5)$  Å). Trace amounts of  $\beta$ -gallium oxide are found only in sample A2 from the unconventional synthesis that used the Inconel reactor and in sample A7. In sample A3 (aerosol generation from a DMF solution), small quantities

(15) Xu, F.; Xie, Y.; Zhang, X.; Zhang, S.; Liu, X.; Xi, W.; Tian, X. *Adv. Funct. Mater.* **2004**, *14* (5), 464.

**Table 4.** Crystalline Phase Analysis for GaN Powders B1–B5 from Ga<sub>2</sub>O<sub>3</sub> Nitridation (*D* (*hkl*), Average Crystallite Size; *a* and *c*, Hexagonal Lattice Parameters)

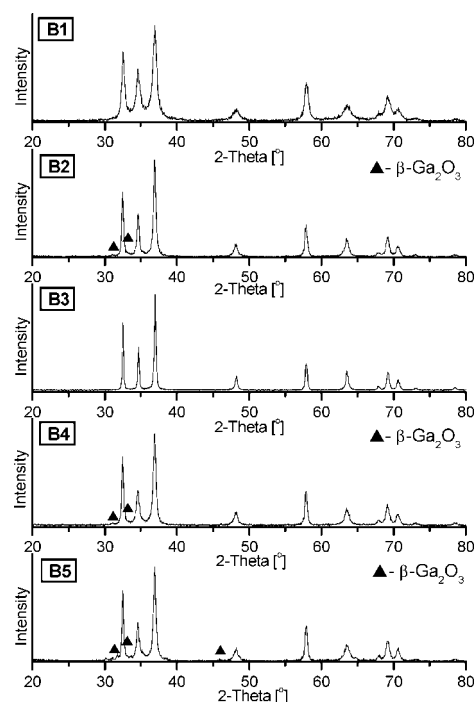
	B1 (comm/900/12)	B2 (comm/950/12)	B3 (comm/975/12)	B4 (aero/400/975/6)	B5 (aero/1050/975/6)
major h-GaN (ordered):	broad	sharp	v. sharp	sharp	sharp
<i>D</i> (100) (nm)	20	39	84	41	43
<i>D</i> (002) (nm)	10	27	60	18	17
<i>D</i> (101) (nm)	13	28	51	24	25
<i>a</i> (Å)	3.1869	3.1882	3.1893	3.1870	3.1863
<i>c</i> (Å)	5.1923	5.1885	5.1873	5.1886	5.1882
residual G <sub>2</sub> O <sub>3</sub>	no	verge of detection	no	verge of detection	7.6 wt %

of the cubic GaN polytype are detected. In the latter case, plausible carbothermal reduction/nitridation processes may have contributed to the formation of c-GaN. Surprisingly, no gallium oxide is detected by XRD in powders A5 and A6 that by elemental analysis contain significant quantities of oxygen, i.e., 4.5 and 2.9 wt %, respectively, and the patterns misleadingly suggest the exclusive presence of the nanocrystalline h-GaN phase. The observation should be traced to a large width of the diffraction peaks for these powders due to small GaN/Ga<sub>2</sub>O<sub>3</sub> crystallite sizes that cause overlapping of the small intensity and broad peaks for the postulated nano-oxide. This situation can be compared to the XRD results for well-crystallized powder B5 (vide infra, Table 4) where the 3.8 wt % O-content is clearly detected in the form of β-Ga<sub>2</sub>O<sub>3</sub> and for powder B1 comparable in crystal characteristics with powder A6, with the former showing the 4.2 wt% O-content and no XRD-detected oxide phase. A detailed curve-fitting analysis of the broad diffraction peaks for powders A5, A6, and B1, however, provides solid evidence that the nanocrystalline gallium oxide is present in all these cases. On the basis of the comparison of numerous XRD patterns for nano-GaN including those with minimal O contents, in our opinion a simultaneous slight increase of the *c* lattice parameter in all these powders can be linked to an averaged bulk/surface effect in small nanocrystallites rather than involving O- for N-substitution effect, i.e., transient gallium oxynitride formation in the bulk phase,<sup>17a</sup> the latter more likely at high pressures or in thin films phases.<sup>17b–f</sup>

The crystallite sizes calculated for the (002) and (100) diffractions are referred to the crystallite dimensions along the *c*-axis and perpendicular to it, respectively, indicating a prevailing crystallite shape, whereas the size calculated from the (101) diffraction reflects more of an average grain size characteristics. From the data in Table 3, a platelet-like crystallite morphology is indicated in most cases, being especially visible in the smaller sized powders A4–A7. The powders with the smallest crystallite sizes of GaN estimated from (101), 7 nm for A5 and 10 nm for A6, were synthesized at the lowest temperatures of 900 and 950 °C, respectively, and still contain unconverted gallium oxide reflected in the O contents of 4.5 and 2.9 wt %. Pyrolyses at 975–1000 °C are required in this method to achieve low O contents below 2 wt % down to a few tenths of a percent, however, at the expense of increased crystallite sizes. Generally, it is difficult with the conventional aerosol-assisted method (generation

from aqueous solutions, standard times and temperatures) to obtain powders with the average crystallite sizes significantly below 20 nm and simultaneously showing low residual O contents. Note the outstandingly high crystallite sizes (above 100 nm) for the very ordered h-GaN component in powder A1 from the highest applied pyrolysis temperature of 1000 °C that also shows the smallest residual O content of 0.4 wt %.

Figure 4 includes the XRD patterns for samples B1–B5 from Ga<sub>2</sub>O<sub>3</sub> nitridation and pertinent structure data are presented in Table 4. As in the case of the chemically similar aerosol-assisted synthesis, all powders appear to be composed mainly of the well-crystallized h-GaN. Of the three closely related powders B1–B3 that were pyrolyzed at the increasing temperatures of 900, 950, and 975 °C, respectively, only the pattern for B2 (O, 1.7 wt %) shows some β-Ga<sub>2</sub>O<sub>3</sub> at the detection limits of the method. As previously discussed, the broad diffraction lines for B1 (O, 4.2 wt %) include overlapping of the low intensity and broad oxide diffractions by the strong peaks for h-GaN. The decreasing O-contents from B1 to B2 to B3 (Table 1) are consistent with improved nitridation conditions at the highest temperatures in the 950–975 °C range. This trend is followed by increased crystallite sizes for the powders, i.e., *D* (101) of 13, 28, and 51 nm, respectively. The worst nitridation circumstances

**Figure 4.** XRD patterns for GaN powders B1–B5 from Ga<sub>2</sub>O<sub>3</sub> nitridation synthesis.

(16) (a) Balkas, C. M.; Basceri, C.; Davis, R. F. *Powder Diffr.* **1995**, *10* (4), 266. (b) Paszkowicz, W.; Podsiadło, S.; Minikayev, R. *J. Alloys Compd.* **2004**, *382*, 100, and references therein.

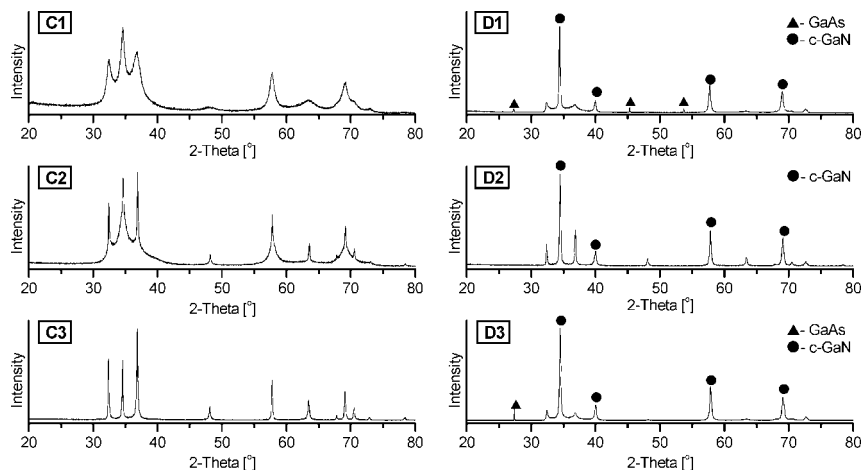


Figure 5. XRD patterns for GaN powders from anaerobic synthesis, C1–C3 (left), and from GaAs nitridation synthesis, D1–D3 (right).

Table 5. Crystalline Phase Analysis for GaN Powders from Anaerobic Synthesis, C1–C3, and from GaAs Nitridation Synthesis, D1–D3 ( $D$  ( $hkl$ ), Average Crystallite Size;  $a$  and  $c$ , Hexagonal Lattice Parameters;  $a$ , Cubic Lattice Constant for Powders D1–D3; u/d, Unable to Determine)

	C1 (600/16)	C2 (700/4/vac)	C3 (975/4/vac)
exclusive h-GaN (defected):	broad	broad	sharp
$D$ (100) (nm)	21	u/d	77
$D$ (101) (nm)	11	40	50
$a$ (Å)	3.193	3.189	3.189
$c$ (Å)	5.197	5.180	5.186
	D1 (700/150/slow)	D2 (800/90/slow)	D3 (800/90/fast)
major I; c-GaN (ordered):	sharp, 55 wt %	v. sharp, 50 wt %	v. sharp, 70 wt %
$D$ (111), nm	60	33	40
$a$ (Å)	4.513	4.506	4.518
major II; h-GaN (defected):	broad, 43.5 wt %	sharp, 50 wt %	sharp, 30 wt %
$D$ (100) (nm)	u/d	68	u/d
$D$ (101) (nm)	n/d	90	u/d
$a$ (Å)	u/d	3.191	u/d
$c$ (Å)	u/d	5.190	u/d
residual c-GaAs	sharp, 1.5 wt %	no	sharp, traces

appear for B4 and B5 because of transient sintering of particles that results in the high O content of 3.8 wt % in B5 after the pyrolysis at 975 °C. This is clearly detected in B5 by XRD in the form of  $\beta$ -Ga<sub>2</sub>O<sub>3</sub>. It is barely detected in B4.

In general, for all powders from the two already discussed related syntheses, a standard interpretation of their XRD spectra suggests the formation of relatively well-crystallized hexagonal gallium nitride as the major product. Only trace quantities of either  $\beta$ -Ga<sub>2</sub>O<sub>3</sub> or c-GaN crystalline phases are sometimes detected. The crystal lattice constants for the h-GaN polytype are within close proximity with the reference literature data and small discrepancies, as frequently done in published reports, can be vaguely explained by crystallite size dependence in the nanosized range and/or by structural defects. At the highest applied pyrolysis temperatures, in most cases h-GaN is the only phase that is characterized by the best crystalline properties (sharp diffraction lines, appropriate line intensities vs microcrystalline reference spectrum, crystal lattice parameters very close to the ones for microcrystalline GaN, etc.). On the basis of such XRD criteria, it is tempting if not common to say that, therefore, good quality nanocrystalline GaN has been synthesized.

The XRD scans for powders C1–C3 from the anaerobic synthesis and for powders D1–D3 from GaAs nitridation are shown in Figure 5 and structural data are included in Table 5. The XRD patterns for C1–C3 show typical products from many anaerobic syntheses, namely, phase inhomogeneous GaN which can be best described as crystallites made of hexagonal and cubic closed-packed layers.<sup>18,9</sup> This is obviously true for nanocrystalline powders C1 and C2 from the pyrolysis temperatures of 600 and 700 °C. At the highest pyrolysis temperature of 975 °C the C3 product is only a slightly defected h-GaN polytype. Because of peak broadness and overlapping, the structural data shown in Table 5 for powders C1 and C2 are only crude estimates of the parameters.

Powders D1–D3 obtained from nitridation of GaAs are all found to contain 50% or more of the cubic polytype of

- (17) (a) Kisailus, D.; Choi, J. H.; Lange, F. F. *J. Cryst. Growth* **2003**, *249*, 106. (b) Lowther, J. E.; Wagner, T.; Kinski, I.; Riedel, R. *J. Alloys Compd.* **2004**, *376*, 1. (c) Soignard, E.; Machon, D.; McMillan, P. F.; Dong, J.; Xu, B.; Leinenweber, K. *Chem. Mater.* **2005**, *17*, 5465. (d) Kroll, P. *Phys. Rev. B* **2005**, *72*, 144407. (e) Ariza, M. J.; Koo, A.; Trodahl, H. J.; Ruck, B. J.; Bittar, A.; Jones, D. J.; Bonnet, B.; Roziere, J.; Moscovici, J. *Surf. Interface Anal.* **2005**, *37*, 273. (f) Tran, N. H.; Lamb, R. N.; Lai, L. J.; Yang, Y. W. *J. Phys. Chem. B* **2005**, *109*, 18348.
- (18) Hwang, J.-W.; Campbell, J. P.; Kozubowski, J.; Hanson, S. A.; Evans, J. F.; Gladfelter, W. L. *Chem. Mater.* **1995**, *7*, 517.

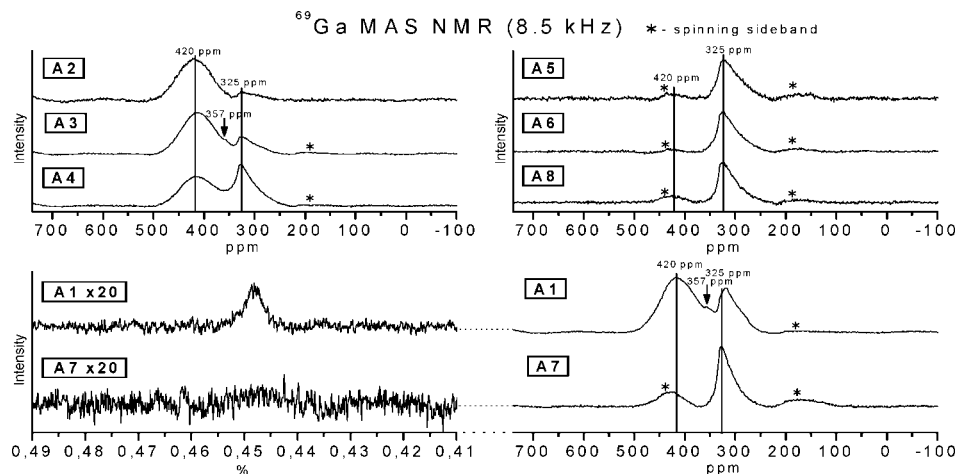


**Figure 6.** Solid-state  $^{69}\text{Ga}$  MAS NMR spectra for GaN powders A1–A8 from aerosol-assisted synthesis.

GaN and the remaining proportion of the defected hexagonal phase of GaN (not marked peaks). Powders D1 and D3 also show ca. 1.5 wt % and traces (preferentially grown) of unconverted GaAs, respectively, indicating experimental difficulties in full nitridation under the applied conditions. The c-GaN polytype appears to be a well-ordered cubic phase with the lattice constant  $a$  in the range 4.506–4.518 Å reported for c-GaN<sup>19</sup> (e.g., ref 19b:  $a = 4.506$  Å) and average crystallite sizes of 33–60 nm. Because of low intensity and overlapping of peaks, it was not possible to determine with sufficient accuracy similar parameters for the defected hexagonal phase in powders D1 and D3.

**Solid-State  $^{69}\text{Ga}$  MAS NMR Characterization.** The  $^{69}\text{Ga}$  MAS NMR spectra for powders A1–A8 from aerosol-assisted synthesis are shown in Figure 6. Note that the spectra for powders A1 and A7, in addition to the common –100–700 ppm acquisition range, were also acquired in the frequency windows appropriate for metallic gallium Knight shift detection.<sup>10</sup> Regarding this, in the high-temperature syntheses of these two powders at 1000 °C, traces of metallic gallium were observed on the crucible's bottom upon powder discharging. Interestingly, the metallic Ga is clearly detected by NMR spectroscopy and supported by XPS data (not shown) in powder A1 although the relevant XRD spectrum does not show its presence (Figure 3). Moreover, for powder A1 the entire magnetic field range from –100 ppm to +0.49% was probed without success for yet other resonances. For these two powders that also display a low intensity broad feature at 100–200 ppm, NMR experiments at variable spinning rates confirmed the feature as the spinning sideband of the major peak at 320–330 ppm and indicated that the associated sideband contributed to the high frequency side of the second resonance at 420–430 ppm.

All the spectra show two basic peaks, namely, at 320–330 ppm and at 415–435 ppm, both positions observed/uncorrected for the second-order quadrupolar shifts, with characteristic shapes and widely varied relative intensities. The relative sharpness and apparent asymmetry of the 320–330

ppm peak, on average 325 ppm, due to mainly second-order quadrupolar interactions is consistent with high grain crystallinity coupled with uniformity of the short-range structure order in the GaN domains responsible for it. A broadened and rather regularly shaped peak at 415–435 ppm contains on the high frequency side an intensity contribution from the spinning sideband of the 325 ppm peak. When this effect is accounted for the average value of 420 ppm can be approximated for this high frequency peak.

The rather scarce literature NMR data for GaN have been interpreted with the notion that the resonance at ca. 325 ppm is for the stoichiometric hexagonal GaN polytype while the broader peak at ca. 420 ppm has been assigned by some researchers either in what appears a rather confusing way to a postulated nonstoichiometric N-deficient phase GaN<sub>1-x</sub> ( $0 < x < 1$ )<sup>4b-c</sup> or, alternatively, in the well-substantiated reports to a Knight shift due to the presence of conduction electrons in the semiconductor.<sup>6</sup> At first glance, the former interpretation of the higher-frequency peak conforms reasonably well with the common knowledge that many high-temperature pyrolyzed GaN powders frequently show by elemental analysis some nitrogen deficiency, while at the same time exhibiting the h-GaN polytype by powder XRD. Following this reasoning and because in the majority of such cases only a single hexagonal pattern for GaN is observed (except for the study by Schwenzer and co-workers<sup>4d,e</sup> mentioned in the Introduction), the concurrent nonstoichiometric nitride phase may have been amorphous in bulk and/or on surface or nanocrystalline in the lowest nanometer range where a long-range order as probed by XRD has no substance. Before further commenting on this issue, we want to add that our detailed analysis of the XRD spectra for all powders discussed in this study ruled out significant quantities of a bulk amorphous phase or a bimodal size distribution that would include large proportions of GaN crystallite fraction in the lowest nanometer range. In the following discussion of the high frequency peak at 420 ppm, we will invoke either an idea of the decomposition-promoted nonstoichiometric N-deficient GaN phase (rather, dopant-stabilized defects of this kind) or the Knight shift involvement whenever they are deemed as consistent with experimental data and both approaches will later be critically confronted.

(19) (a) Purdy, A. P. *Chem. Mater.* **1999**, *11*, 1648. (b) Jegier, J. A.; McKernan, S.; Purdy, A. P.; Gladfelter, W. L. *Chem. Mater.* **2000**, *12*, 1003, and references therein. (c) Jouet, R. J.; Purdy, A. P.; Wells, R. L.; Janik, J. F. *J. Cluster Sci.* **2002**, *13* (4), 469.

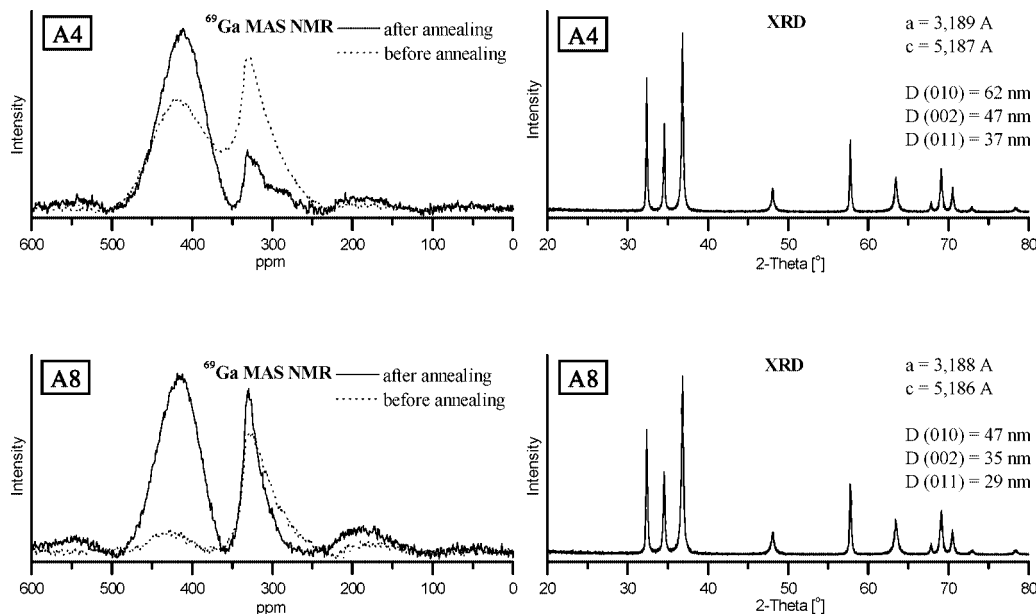


**Figure 7.** Solid-state  $^{69}\text{Ga}$  MAS NMR spectra and XRD patterns for annealed/partially decomposed GaN powders A4 and A8.

In the NMR spectra for powders A1 and A3, an additional small intensity peak at ca. 357 ppm is seen and can be assigned to small quantities of c-GaN.<sup>5</sup> Some cubic GaN is also confirmed in these powders by detailed analysis of the relevant XRD patterns.

Each of the powders A5–A8 shows the prevailing peak at 325 ppm and only a trace peak at 420 ppm suggesting that these materials are mostly composed of the crystalline and stoichiometric h-GaN. This finds a reasonable explanation from the way they were prepared in relation to GaN stability at the temperatures of pyrolysis. Namely, powders A5 and A6 were pyrolyzed for 6 h at the relatively low temperatures of 900 and 950 °C, respectively, under which conditions gallium nitride shows a decent thermal stability, and therefore, the amounts of the presumed decomposition-derived N-deficient phase would be rather small. Completely different mechanism may have operated for powder A8 that was prepared at 975 °C, 6 h, but was later washed/cleaned with an HF solution. On the one hand, these pyrolysis conditions are rough enough to initiate a noticeable GaN decomposition but, on the other hand, washing with a very intrusive HF solution could have preferentially dissolved/removed the compositionally defective nitride phase. It is worth mentioning that in the first paper reporting the specifics of both the  $^{69}\text{Ga}$  NMR and  $^{71}\text{Ga}$  NMR spectroscopy for GaN powders including the broad peak at ca. 450 ppm for the then-proposed (undefined) impurity, its intensity significantly decreased upon washing the powder with aqua regia.<sup>4a</sup> It is also instructive to point out that powders A5–A8 are all characterized with the XRD patterns each showing well-crystallized h-GaN of differing average crystallite sizes (Figure 3, Table 3).

In powders A1–A4, the peak at 420 ppm is significant if not prevailing in relation to the peak at 325 ppm that would support copious amounts of the N-deficient phase, especially in powder A2. On the other hand, there is nothing outstanding in these powders' XRD spectra: they all show patterns for ordered h-GaN. The relatively high average crystallite sizes

here result from the applied high pyrolysis temperatures and can be compared with the appropriate values for the previously discussed powders A7 and A8 that, contrary to powders A1–A4, show the prevailing NMR resonances at 325 ppm.

To directly address the question of progressing GaN decomposition in relation to the evolution of the high frequency peak at 420 ppm, the following experiment was carried out. Powders A4 (both NMR peaks of significant intensities) and A8 (prevailing NMR peak at 1000 °C for 3 h followed by 1050 °C for 5 h, i.e., under conditions forcing noticeable decomposition of GaN and darkening of the materials. Figure 7 includes the comparative  $^{69}\text{Ga}$  MAS NMR spectra (left) and the XRD scans and derived hexagonal lattice parameters/crystallite sizes (right) for the annealed powders. The NMR spectra for both annealed powders clearly show increased proportions of the 420 ppm peak at the expense of the 325 ppm peak. At the same time, the hexagonal polytype persisted and refined while the average crystallite sizes in both cases increased relative to the initial powders (compare these XRD data with those in Table 3). Undoubtedly, slowly progressing decomposition of GaN forms a basis for the evolution of the high frequency NMR peak at 420 ppm while, simultaneously, the XRD long-range order improved characteristics appear to result from concomitant grain growth/recrystallization of the GaN particles.

The NMR spectra for powders B1–B5 from the  $\text{Ga}_2\text{O}_3$  nitridation synthesis are displayed in Figure 8. The specific feature here is the high frequency side resonance shifted slightly toward higher frequencies within the 420–450 ppm range and at least part of this shift could be attributed to the peak's overlapping with the spinning sideband of the 325 ppm peak. In the series of closely related powders B1–B3, only powder B1 from the lowest pyrolysis temperature of 900 °C has a predominant 325 ppm peak. Powders B2 and B3 from the higher pyrolysis temperatures show increased proportions of the 420 ppm peak and 450 ppm peak,

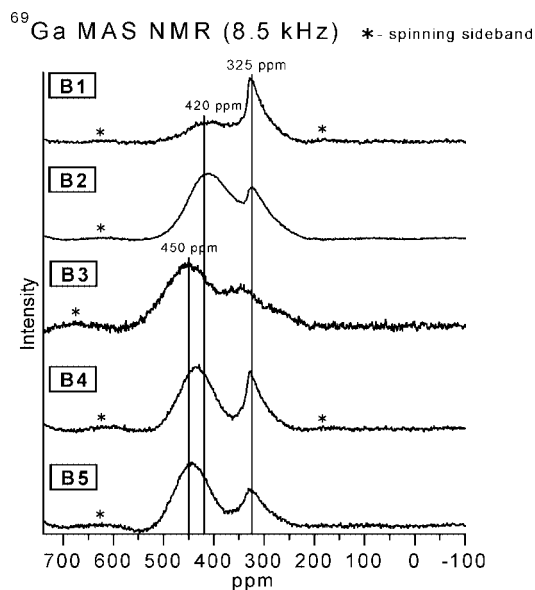


**Figure 8.** Solid-state  $^{69}\text{Ga}$  MAS NMR spectra for GaN powders B1–B5 from  $\text{Ga}_2\text{O}_3$  nitridation synthesis.

respectively, while their XRD scans display better crystallinity than for powder B1, thus confirming a similar trend as observed among powders from the aerosol-assisted method. It appears that the application of different pyrolysis times in these two chemically similar methods causes faster recrystallization and decomposition phenomena in the  $\text{Ga}_2\text{O}_3$  nitridation system (12 h) than in the related aerosol-assisted synthesis (6 h) as can clearly be seen from comparison of the NMR and XRD spectra for powders A6 and B2 pyrolyzed at the same temperature of 950 °C.

The left-hand part of Figure 9 contains the  $^{69}\text{Ga}$  MAS NMR spectra for powders C1–C3 from the anaerobic synthesis. Powders C1 and C2 from the lowest pyrolysis temperatures of 600 and 700 °C, respectively, are each characterized by a single NMR peak at 325 ppm (stoichiometric h-GaN). On the other hand, the NMR spectrum for powder C3 pyrolyzed at 975 °C is dominated by a strong and broad peak at 420 ppm complemented by a weak peak at 325 ppm. The specific feature of the anaerobic synthesis in comparison to both the aerosol-assisted and  $\text{Ga}_2\text{O}_3$  nitridation syntheses is a possibility to prepare nanopowders of GaN at significantly lower temperatures while of structurally defected hexagonal polytype.<sup>9,18</sup> The XRD patterns for powders C1 and C2 show the broad diffractions typical for a strongly defected h-GaN, whereas for C3, the pattern is typical for only a slightly defected h-GaN polytype (Figure 5, Table 5). These interpretations are in good agreement with the available TGA stability data (Table 2). The thermal decomposition of powder C2 takes place at 930 °C, much higher than the 700 °C pyrolysis temperature for the powder, and therefore, no clear signs for the presumed N-deficient phase from h-GaN decomposition are observed by NMR. On the other hand, powder C3 was prepared at 975 °C close to the 1050 °C decomposition temperature of this material, i.e., temperature high enough to have resulted in significant N-deficient phase formation.

The right-hand part of Figure 9 shows the  $^{69}\text{Ga}$  MAS NMR spectra for powders D1–D3 prepared via GaAs

nitridation. A quantitative comparison of the relative intensities in these standard spectra is rather equivocal since the effective tilting angle in the NMR experiment is different for the hexagonal and cubic phases. A relatively narrow line at 215 ppm<sup>4a,5b</sup> indicates some unconverted GaAs in powder D1 and merely traces of it in powders D2 and D3. This is in a qualitative agreement with the relevant XRD patterns although no GaAs at all is detected by XRD in powder D2 (Figure 5). It is appropriate to recall at this point that these powders are composite mixtures of two major components, namely, cubic and hexagonal GaN polytypes (Table 5).

The best quality powder D2 (ca. 50/50 of c-GaN/h-GaN) displays a complex NMR spectrum with four overlapping resonances in the nitride range. On the lower-frequency side, there are two medium intensity and relatively sharp peaks at 325 and 357 ppm that can be linked to the stoichiometric h-GaN and c-GaN polytypes, respectively. The very broad peak centered at 420 ppm can be associated with the presumed N-deficient phase originating from hexagonal GaN, as discussed earlier. However, the strongest and sharper peak at ca. 470 ppm is a new feature in this study. By analogy with the pair of peaks at 325 and 420 ppm linked to the hexagonal polytype, we tentatively suggest that the peak at 470 ppm reflects yet another N-deficient phase derived this time from cubic GaN. It is interesting to refer now to this powder thermal stability by TGA/DTA as the decomposition temperature of 1040 °C (Table 2). The powder was synthesized at 800 °C, i.e., much below its decomposition temperature; but despite this, the NMR spectrum shows significant amounts of the presumed N-deficient phases. This can be understood in terms of the extremely long pyrolysis time of 90 h to be compared with the nonequilibrated conditions of fast heating (10 °C/min) in the TGA/DTA experiment. It appears, therefore, that nanosized GaN powders can undergo significant changes already at 800 °C if sufficiently long heating times are applied.

The NMR spectrum for powder D1 shows an asymmetric peak at 325 ppm (stoichiometric h-GaN) and a broad and slightly asymmetric (due to a spinning sideband presence) line on the high frequency side at 470 ppm (N-deficient phase from c-GaN) with no significant intensity around 420 ppm (N-deficient phase from h-GaN). In this regard, this powder was synthesized at the lowest temperature of 700 °C, much below GaN decomposition temperatures for these materials. Interestingly, the NMR spectrum suggests that under these conditions (700 °C, 150 h) the crystalline h-GaN is more stable than the crystalline c-GaN because the peak at 470 ppm assigned to the N-deficient phase from decomposition of c-GaN and the peak at 325 ppm for the stoichiometric h-GaN dominate.

Powder D3 was synthesized under similar conditions as powder D2 differing mainly by a significantly higher ammonia flow during the synthesis of the former. Interestingly, this results in the NMR spectrum for D3 showing almost exclusively the band of lines for the N-deficient phases with the major peak at 470 ppm and a shoulder at ca. 420–430 ppm and only traces of lines if any for the stoichiometric phases. This suggests that under the applied pyrolysis conditions, cubic GaN was preferentially formed

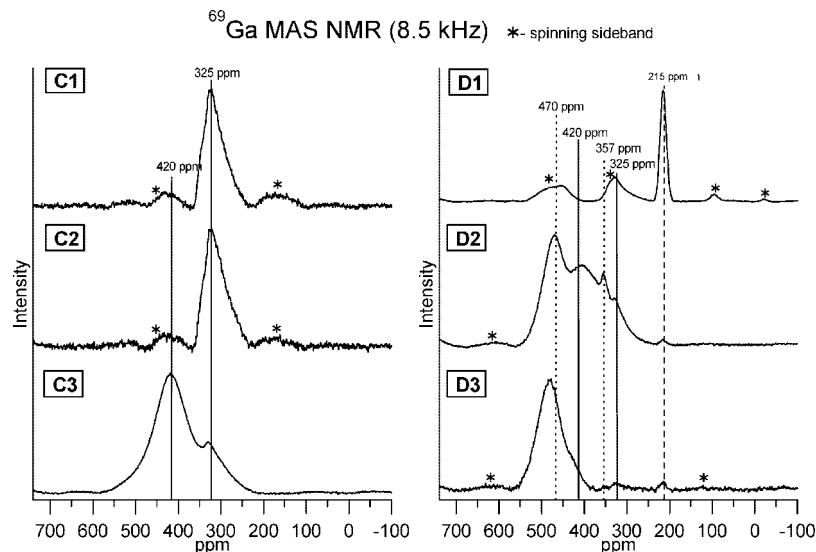


**Figure 9.** Solid-state  $^{69}\text{Ga}$  MAS NMR spectra for GaN powders from anaerobic synthesis, C1–C3 (left) and from GaAs nitridation synthesis, D1–D3 (right).

and later significantly decomposed. This is further supported by XRD that confirms the prevailing c-GaN.

**N-Deficiency-Related Defects vs Knight Shift Effect in GaN Powders.** The only apparent correlation observed in this study among the GaN powders between the specifics of the XRD patterns and NMR spectra is that the high temperature promoted better crystallinity of the given polytype is accompanied by increased proportions of the NMR peak appearing in the 420–450 ppm range for h-GaN or at ca. 470 ppm for c-GaN, somewhat counter-intuitively if the shifts would have to be associated with distinct decomposition phases. At the same time, as already mentioned, a careful analysis of the XRD spectra shows no signs of significant proportions of a bulk amorphous phase and/or nanometric phase in the lowest nanosized range that could be related to the additional distinct phase implied by NMR in any of the samples. We want to point out, however, that the powders constitute a size-heterogeneous system of which particle sizes, crystalline properties, and surface vs core characteristics are averaged out by powder XRD data. Therefore, the observed bimodal NMR response for each polytype can be linked, for instance, to different particle sizes/size ranges or to particle surface vs core domains, each case yielding under certain circumstances a single XRD pattern.

Considering again the assignments of the gallium NMR spectra, the low frequency ca. 325 and 357 ppm line positions for h-GaN and c-GaN, respectively, seem to be well-documented and accepted for a range of GaN materials in the sense that they are related to four-coordinated gallium Ga(4N) chemical environments as expected in both stoichiometric polytypes. The assignment of the corresponding peaks at 420–450 ppm (h-GaN) and 470 ppm (c-GaN), i.e., significantly shifted toward higher frequencies by some 100 ppm or more vs. the respective stoichiometric phase peaks, at first glance, can misleadingly suggest the existence of some stable three-coordinated Ga(3N) domains resulting from partial decomposition with nitrogen depletion. For instance, the decrease in gallium coordination number from 6 to 4 in two different environments in  $\beta\text{-Ga}_2\text{O}_3$  causes a high

frequency shift of the gallium NMR line by some 160 ppm from ca. 40 ppm (6-coordinate) to 200 ppm (4-coordinate)<sup>20a</sup> and similar shifts are observed for various 6-, 5-, and 4-coordinated gallium–oxygen compounds.<sup>20b,c</sup> However, a quantitative evaluation of the relative proportions of the Ga nuclei linked to the high-frequency NMR peak in relation to the characteristics of the related XRD data as well as the fact that the chemically unlikely 3-coordinated gallium centers would almost certainly have an enormous quadrupole coupling constant and hence broaden a resulting NMR resonance beyond detection rule out a simple structural N-deficient Ga(3N)-center effect, i.e., 3-N-coordinated Ga chemical environments to be directly responsible for the high-frequency peak. There must be instead another factor crucially contributing to the shift while related to the N-deficiency.

We think that our observations can be reasonably accounted for under two restrictions. First, from the composition/structure point of view, we have to assume that the proposed by others and consistent with this study high temperature-induced sites in GaN such as some stable non-Ga(4N) centers, e.g., 4-coordinated Ga(3N)(X), where X is a stabilizing foreign atom (likely, X = O or H), are in sufficiently low quantity and random distribution throughout the bulk of GaN crystallites or in surface layers as to not influence significantly the stability and long-range order of the GaN lattice as substantiated by the XRD data. Some potential in addressing this problem in a quantitative way may reside in calculations of properties and energetic stability of various native (compositional) defects in GaN.<sup>21</sup> Recent data of this kind support, for instance, a preferential formation of N-defects, their increased concentration and mobility with

(20) (a) Massiot, D.; Farnan, I.; Gautier, N.; Trumeau, D.; Trokner, A.; Coutures, J.-P. *Solid State Nucl. Magn. Reson.* **1995**, *4*, 241. (b) Bradley, S. M.; Howe, R. F.; Kydd, R. A. *Magn. Reson. Chem.* **1993**, *31*, 883. (c) Ash, J. T.; Grandinetti, P. J. *Magn. Reson. Chem.* **2006**, *44*, 823.

(21) For example, see (a) Ganchenkova, M. G.; Nieminen, R. M. *Phys. Rev. Lett.* **2006**, *96*, 196402, and references therein. (b) Van de Walle, C. G.; Neugebauer, J. *J. Appl. Phys.* **2004**, *95* (8), 3851.

temperature, and localized nature of associated electrons within the radius encompassing the second nearest neighbors,<sup>21a</sup> whereas others stress the importance of contaminant oxygen or hydrogen atoms on defect formation and stabilization.<sup>22,23</sup> As a matter of fact, defect stabilization by oxygen seems to be highly probable here given the nature of the applied precursors (O-bearing gallium compounds in two syntheses) and common ammonia reactant contaminations (traces of water vapor and oxygen). The inferred from several studies gradual decomposition of GaN with nitrogen depletion at appropriately high temperatures/long heating times could thus be associated with the formation of 4-coordinated Ga(3N)(O) defects (oxygen incorporation into the GaN lattice). In this regard, the powders prepared at lower temperatures contain on average smaller crystallites (XRD) of apparently highly stoichiometric composition reflected in the predominant Ga(4N) chemical environments (NMR). Higher synthesis/annealing temperatures, especially, coupled with extended treatment times result in larger and better-ordered (XRD) while more defected (NMR) crystallites, the latter phenomenon enhanced by the nitride's lattice instability and recrystallization/crystal growth phenomena.

Second, and crucially, we have to accept that crystallites or domains with such native compositional defects exhibit unique electronic properties with a specific gallium NMR response. In this regard, a plausible shallow donor oxygen dopant in such defects could be a source of conduction electrons and resultant new "electronic phase".<sup>22,23</sup> We would like to recall that similar kind of the electronic phase associated with a specific Knight shift in semiconductors due to conduction electrons in both intentionally (e.g., 0.13 wt % Ge) and unintentionally doped GaN has recently been proposed and well substantiated by Yesinowski et al.<sup>5a,6</sup> As a matter of fact, the <sup>71</sup>Ga MAS NMR spectrum for their Ge-doped GaN powder resembles closely our NMR spectra for powders A3 (Figure 6) or C3 (Figure 9) by showing the prevailing peak at ca. 440 ppm (Knight shift effect) and a smaller intensity and sharper peak at 330 ppm (stoichiometric h-GaN).<sup>6b</sup> The similarity of their NMR spectra to our results suggests that the specific electronic phase and associated conduction electrons are intrinsically common in many if not all high-temperature-synthesized or annealed intentionally pure GaN powders.

In summary, it seems coherent to directly link the formation of the thermally induced foreign atom stabilized N-deficient domains/native N-vacancies in the pure GaN nanopowders with the presence of conduction electrons responsible for the Knight shift effect in the NMR spectra. From a different angle, the NMR spectroscopy in combination with XRD measurements and TGA/DTA stability data

offer an invaluable insight into, apparently, a gradual transition from the stoichiometric with no conduction electrons (exclusive 325 ppm peak for h-GaN or 357 ppm peak for c-GaN) to the nonstoichiometric with conduction electrons (exclusive 420–450 ppm peak for h-GaN or 470 ppm peak for c-GaN), whereas well-crystallized pure GaN powders from high-temperature/long-time treatments. A more detailed analysis of peak broadening and variations in peak positions will be necessary to relate the Knight shift evolution to the particle size and/or particle surface vs core nonuniformities in the powders.

## Conclusions

Nineteen GaN powders prepared by four synthesis methods constituted a comprehensive materials stage for the study of short/long-range structural and electronic properties related to the powders' thermal stabilities. These materials showed by XRD diffraction crystalline GaN polytypes encompassing the single ordered or defected hexagonal GaN and composite mixtures of the ordered cubic and defected hexagonal GaN to yield, with increasing pyrolysis or annealing temperatures, materials of better crystallinity and larger average crystallite sizes. At the same time, no significant amounts of amorphous or nanocrystalline GaN domains in the lowest nanosized range were detected while metallic gallium was occasionally observed. The <sup>69</sup>Ga MAS NMR spectroscopy for the powders provided two peaks with varying relative intensities for each GaN polytype. The high-frequency shifted peak was related to the decomposition-induced N-deficient domains and dominated over the low frequency peak for stoichiometric GaN after higher pyrolysis temperatures and/or extended pyrolysis times. The XRD-derived features had a general correlation with the corresponding NMR data in that the better crystallinity corresponded with the evolution and increased proportions of the NMR high frequency peak. This trend could be satisfactorily accounted for by assuming that the rather scarce N-deficient sites (e.g., oxygen dopant stabilized defects or native N-defects) resulting from partial decomposition of GaN form a structural basis for the electronic phase with conduction electrons, the latter causing the Knight shift effect in gallium NMR and, therefore, significantly altering many materials properties. The knowledge of the trends in formation and proportions of the two different phases, both being the function of powder thermal stability in relation to the temperature/time history of synthesis or annealing, will be crucial in appraising GaN powder suitability for many high-temperature applications.

**Acknowledgment.** J.F.J. acknowledges the support of the Polish Ministry of Science and Higher Education/AGH-UST, Grant 11.11.210.120. R.T.P. acknowledges support from the U.S. National Science Foundation (Grant CHE-9983205) for the U.S.–Polish collaboration.

CM800645Q

(22) For example, see (a) Kikkawa, S.; Nagasaka, K.; Takeda, T.; Bailey, M.; Sakurai, T.; Miyamoto, Y. *J. Solid State Chem.* **2007**, *180*, 1984. (b) Wright, A. F. *J. Appl. Phys.* **2005**, *98* (10), 103531. (c) Wright, A. F.; Seager, C. H.; Myers, S. M.; Koleske, D. D.; Allerman, A. A. *J. Appl. Phys.* **2003**, *94* (4), 2311.

(23) Sheu, J. K.; Chi, G. C. *J. Phys.: Condens. Matter* **2002**, *14*, R657.